ACS SENSORS

Article

pubs.acs.org/acssensors

# Sensing Hydrogen Gas from Atmospheric Pressure to a Hundred Parts per Million with Nanogaps Fabricated Using a Single-Step Bending Deformation

Eredzhep Menumerov,[†] Bryan A. Marks,[†] Dmitriy A. Dikin,[†] Francis X. Lee,[†] Robert D. Winslow,[†] Saurav Guru,[†] Devika Sil,[‡] Eric Borguet,[‡] Parsaoran Hutapea,[†] Robert A. Hughes,[†] and Svetlana Neretina*[,†]

[†]College of Engineering and [‡]Department of Chemistry, Temple University, Philadelphia, Pennsylvania 19122, United States

Supporting Information

**ABSTRACT:** The widespread use of $H_2$ gas as an energy carrier will necessitate the development of inexpensive, easily manufactured sensors which reliably monitor gas levels where $H_2$ is used, transported, and stored. Nanogap sensors transduce the volume expansion which accompanies hydrogen uptake by palladium-based metal-hydrides into an electrical signal through the closure of nanogaps which allows a previously interrupted current to flow. While this break-junction design offers numerous functionalities, limitations still exist in terms of fabricating nanogap sensors responsive to a wide range of partial pressures. Here, we invoke a detection strategy where up to 10 000 nanogaps of various widths act in concert to provide an overall analog signal which continuously varies as the $H_2$ partial pressure is varied from a hundred parts per million to 1 atm. The sensor is fabricated by mechanically coupling an AuPd film to a support consisting of polyimide, an adhesive, and a steel backing which, when bent, forms parallel cracks in the film which act as nanogaps. With characteristics that include room temperature detection, a high sensitivity and selectivity toward $H_2$, low-cost lithography-free fabrication, recyclability, low power consumption, simple circuitry, and favorable aging characteristics, the device meets many of the criteria needed for practical $H_2$ sensing.

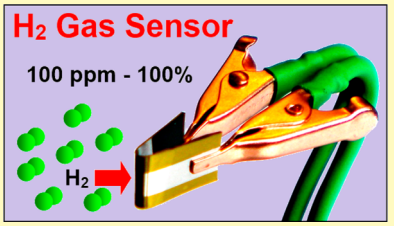


**KEYWORDS:** *nanogap sensor, hydrogen, bending deformation, AuPd, cracks, polyimide*

Diatomic hydrogen is a colorless, odorless, and tasteless gas which, when combined with air, poses a safety hazard due to its wide flammability range (4−75%) where high burning velocities and explosive tendencies compound the risks.[1,2] At high concentrations it can also act as an asphyxiant. Its importance stems primarily from its use as a reactant for the chemical industry in the processing of ammonia, petrochemicals, and methanol. It also finds uses as an energy carrier, with notable applications in fuel cell technologies and rocket propulsion systems. With renewed emphasis being placed on the production of $H_2$ through photocatalytic water splitting,[3−7] the advancement of a hydrogen economy powered by sunlight seems more probable. Moreover, $H_2$, derived from renewable sources of clean energy, also has the potential to act as a feedstock for reactions which transform sequestered $CO_2$ back into a useable fuel through catalytic hydrogenation,[8−10] an approach which not only yields fuels with a greater energy density than $H_2$, but also consumes a damaging greenhouse gas. If such an energy infrastructure is to emerge then it will inevitably be monitored by a network of sensing devices which detect $H_2$ levels where it is used, transported, and stored.[11−17] If, in this scenario, distributed $H_2$ power generation systems become commonplace, then such point-of-use consumption could eventually make $H_2$ sensors as ubiquitous as carbon monoxide and smoke detectors.

While numerous commercial $H_2$ sensors already exist, none of them meet all of the performance criteria demanded by the diverse range of existing and future applications.[18] In response to this unmet need a wide variety of sensors have been recently prototyped which are reliant on nanostructured materials as the active sensing element.[12] Prominent examples include those based on (i) the closure of nanogaps,[11,19] (ii) alterations to the plasmonic resonance of noble metal nanostructures,[13,20−22] (iii) resonant shifts in surface acoustic wave (SAW) devices,[23−25] (iv) alterations to the optical or transport properties of semiconductor oxide nanostructures,[14,16] and (v) carbon-based nanostructures (e.g., carbon nanotubes, graphene) functionalized for $H_2$ detection.[26−28] Of specific relevance to this work is the nanogap strategy, which is reliant on the volume expansion occurring when $H_2$ dissociation on the surface of Pd leads to its rapid absorption. This sensing strategy, devised by Penner and co-workers,[19,29] demonstrated a break-junction design whereby electrical contact between adjacent mesoscopic Pd wires could be enabled or disabled depending on whether these structures swelled in the presence of $H_2$ to form a closed circuit or contracted when $H_2$ desorbed to form an open circuit where the width of the nanogap

**Received:** September 11, 2015
**Accepted:** October 22, 2015
**Published:** October 22, 2015





DOI: 10.1021/acssensors.5b00102
*ACS Sens.* 2016, 1, 73−80

determined the $H_2$ partial pressure needed to actuate the device. These sensors were advantageous in that they showed far greater sensitivity than conventional Pd-based sensors[30] which have a detection mechanism based on the dependency between the $PdH_x$ resistance and its hydrogen content.

Since the initial nanogap device demonstration, significant advancements have been made to this sensing platform. There now exist numerous schemes for nanogap fabrication utilizing both sophisticated lithographic methods[31−37] and routes directed toward the advancement of the inexpensive devices[38−49] which are often preferred by sensor manufacturers. Nanogap sensors can be operated as (i) an on−off switch where the nanogap spacing is targeted toward a specific $H_2$ concentration, (ii) a device sensitive to a broad range of $H_2$ concentrations through the use of a percolative electrical pathway between closely spaced nanostructures where the ensemble becomes less resistive as more nanogaps close, or (iii) a hybrid sensor reliant on using one of the aforementioned nanogap sensing modes in combination with the conventional Pd sensing strategy reliant on the $PdH_x$ resistance. While the hybrid approach aims to increase the sensing range, its effectiveness is limited by the fact that these two sensing mechanisms act in opposition, with nanogaps decreasing the overall resistance at higher $H_2$ concentrations and the $PdH_x$ resistance increasing it. The hybrid strategy, therefore, utilizes the $PdH_x$ resistance as an effective means of detection once all of the nanogaps have closed, but is otherwise deleterious to sensor sensitivity. This work has also given rise to a number of breakthroughs which have come to benefit the overall sensing platform, most notable of which is the effectiveness of using polymeric materials such as polyimide (Kapton)[31,40] or polydimethylsiloxane (PDMS)[38,39] as a compliant elastomeric substrate able to accommodate the local strains that occur as Pd expands and contracts while maintaining the integrity of the interface and, hence, allowing for atypical volume expansions[31] while inhibiting Pd delamination. Another advance of note is the demonstration of sensor performance gains available when using Pd alloys.[38]

Despite the many successes, numerous challenges still remain in terms of advancing nanogap sensors as a commercially viable option for $H_2$ detection. Broad range detection, for example, requires that a single sensor contain a continuum of nanogap spacings which sequentially close as the $H_2$ concentration is increased. Extending the low detection limit to smaller values requires the formation of sub-20 nm gaps whose fabrication presents technical challenges.[11] Extending the high detection limit faces hurdles in terms of providing a Pd−substrate interface which resists delamination without excessively frustrating the large volume expansions needed to close wide nanogaps. Between these two extremes must exist a large number of nanogaps with variable spacings able to provide an overall signal which continuously varies between the low and high detection limits. Here, we demonstrate that a simple single-step bending deformation performed on an AuPd film deposited on a mechanically compliant substrate induces up to 10 000 partial cracks which, when exposed to hydrogen, act as a room temperature nanogap sensor able to reversibly detect $H_2$ partial pressures in a range extending from a hundred parts per million to 1 atm. With nanogap sensitivity at high $H_2$ concentrations exceeding that obtainable through changes to the $AuPdH_x$ resistance, the sensing strategy eliminates the need for hybrid sensing modes and, hence, allows for a full-range nanogap sensor reliant on a single sensing mechanism.

## EXPERIMENTAL SECTION

**Chemicals and Materials.** The active sensing material was derived from a $Au_{0.5}Pd_{0.5}$ sputter target with 99.99% purity. It is supported by various substrate and backing materials which include Kapton tape (TapeCase Ltd.), cold-rolled low carbon steel foil, and Teflon (polytetrafluoroethylene). Sensor performance was assessed using ultrahigh purity $H_2$ and mixtures of $H_2$ and an inert carrier gas (either $N_2$ or Ar depending on availability).

**Hydrogen Gas Sensing.** The electrical resistance of the sensor, which functions as a two terminal ohmic device, was recorded at a sampling rate of 60 $s^{-1}$ using a voltage divider circuit with a 1 V DC bias. Prior to $H_2$ exposure, sensors were monitored to establish a stable baseline resistance. For the recyclability and aging experiments the sensors were housed in an airtight chamber through which $H_2$ and inert carrier gases were flowed at a rate of 500 $cm^3$/min. The volume of the chamber is approximately 200 $cm^3$. Experiments, which assessed the sensor response as a function of $H_2$ concentration, were carried out in a separate chamber which allowed all air to be evacuated prior to the exposure of the sensor to $H_2$/carrier gas mixtures. This chamber allowed for the rapid exposure (∼1 s) of the sensor to the gas test mixture since the purging of air from the system was not involved and, as a result, provided sensor response times closer to their intrinsic values.

**Instrumentation.** $Au_{0.5}Pd_{0.5}$ films were sputter deposited using a Model 681 Gatan High Resolution Ion Beam Coater at a rate of 7 nm/min in a vacuum chamber with a base pressure of $1 \times 10^{-6}$ Torr. Images were acquired with an FEI Quanta 450 FEG SEM environmental scanning electron microscope using the secondary electron detector. The electrical response of sensors was monitored using LabVIEW System Design Software interfaced to a data acquisition system (National Instruments).

## RESULTS AND DISCUSSION

**Sensor Fabrication.** The hydrogen gas sensor is a four layer device consisting of an $Au_{0.5}Pd_{0.5}$ alloy thin film, a polyimide substrate, an adhesive, and a steel backing. Figure 1 shows both a schematic representation of the process used to fabricate the sensor as well as an image of the device. It begins with the placement of a strip of Kapton tape consisting of a 60-$\mu$m-thick layer of polyimide backed with an adhesive onto a steel foil substrate with dimensions of $25 \times 5 \times 0.127$ $mm^3$ (Figure 1a). An AuPd film is then sputter deposited onto the Kapton at room temperature through a shadow mask with a $25 \times 3$ $mm^2$ rectangular opening to a thickness of 90 nm (Figure 1b). The four layer structure is then bent around a metal rod with a 1 mm radius of curvature (Figure 1c). The deformation leads to the formation of cracks in the AuPd film which serve as nanogaps responsive to $H_2$ exposure. When the mechanical force is released the sensor retains a bent shape with an overall height of approximately 10 mm. Electrical contacts are then added to each end of the sensor to facilitate two-probe resistance measurements (Figure 1d). The process is straightforward, lithography-free, and can be carried out in less than 15 min with material costs of less than 15 cents. The simple inexpensive design and the ease of fabrication represent key advantages of this approach.

The four layer sensor design is the product of earlier prototypes which led to an understanding of the role which each layer plays in both device fabrication and performance. The AuPd alloy was chosen as the active $H_2$ sensing material instead of elemental Pd since the latter is prone to (i) delamination from the substrate material due to interfacial strains resulting from the abrupt volume change which occurs as it undergoes an $\alpha$- to $\beta$-phase transition at low $H_2$ concentrations[50] and (ii) surface poisoning when exposed to


DOI: 10.1021/acssensors.5b00102
ACS Sens. 2016, 1, 73−80

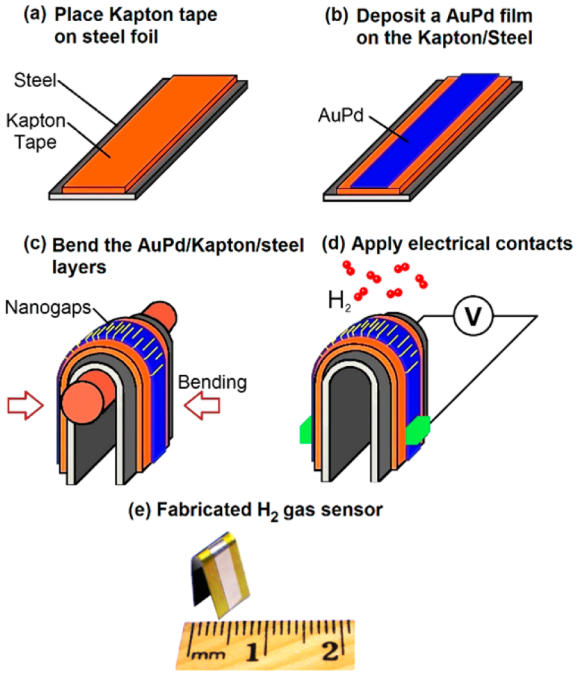


**Figure 1.** Schematic showing the sensor fabrication process. The process proceeds by (a) placing a strip of Kapton tape (i.e., polyimide and an adhesive) onto a steel foil substrate, (b) sputter depositing an AuPd strip onto the Kapton through a shadow mask, (c) inducing nanogaps into the AuPd strip through a bending deformation around a known radius of curvature, and (d) attaching electrical contacts to the AuPd. (e) $H_2$ nanogap sensor shown next to a ruler with mm markings for scale.

low concentrations of $H_2S$ and CO over extended time intervals.[30,51] While the active AuPd layer is of obvious importance to device operation, the polyimide, adhesive, and steel layers derive significance beyond acting as a mere support for the sensing element. When bent, the four layers which comprise the sensor are mechanically coupled to one another. During this process the steel is plastically deformed, the result of which is an irreversible deformation that maintains nanogap spacing and preserves the shape of the sensor. It also provides an overall rigidity to the bent structure which leads to a sensor which is more robust and comparatively insensitive to vibrations. The Kapton tape acts as a flexible substrate able to both electrically isolate the AuPd layer and diminish the interfacial tensions occurring during both the bending deformation and as the AuPd crystal structure undergoes repeated expansion−contraction cycles due to $H_2$ absorption and desorption.

**Nanogap Formation and Characterization.** Prior to bending, a 90-nm-thick AuPd film has a near-featureless surface and a resistance of approximately 30 Ω. The bending deformation results in an increase in the resistance of several hundred ohms, a value which becomes the baseline resistance ($R_0$) of the sensor. An examination of the AuPd surface morphology reveals approximately 10 000 near-parallel cracks running normal to the direction of net current flow. The increased resistance, hence, originates from the meandering path which the electrons must now travel in order to traverse the length of the sensor. Figure 2a−c shows SEM images of these cracks at various magnifications. The histogram in Figure 2d reveals crack lengths extending up to 450 $\mu$m with an average center-to-center spacing of 10.3 $\mu$m. Important to note is that, in no case, does a crack extend across the 3 mm width of the sensor. Instead, each crack shows a fairly consistent width in the range 30 to 200 nm (Figure 2d) along most of its length, which then rapidly narrows to a point of closure followed by a short length which is cracked, but where no discernible gap is apparent (Figure 2c). Collectively, these features consist of a continuum of nanogap spacings, each sensitive to a different $H_2$

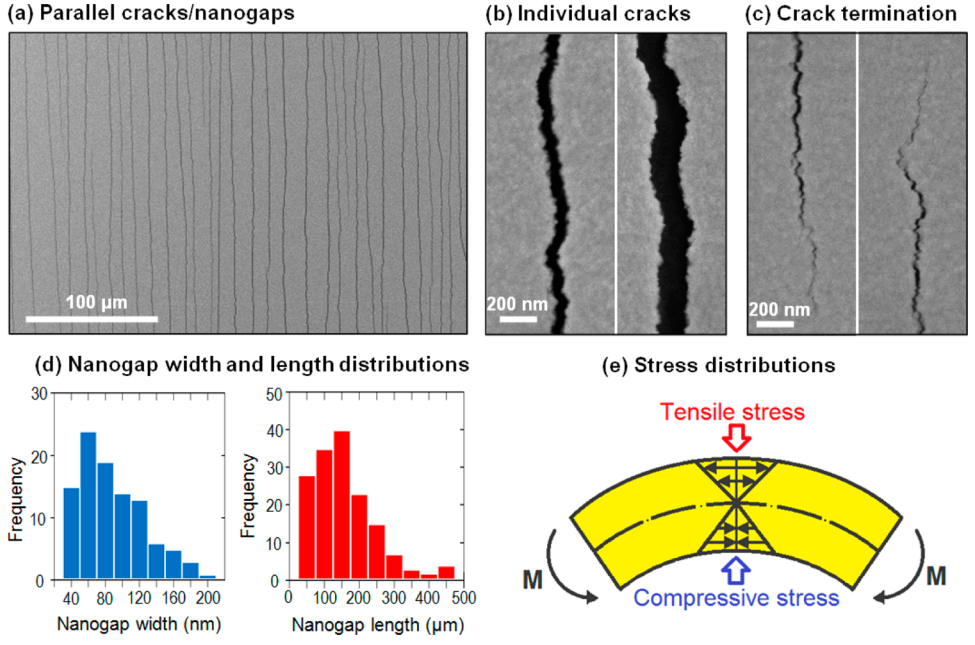


**Figure 2.** SEM images showing (a) many parallel cracks/nanogaps in the AuPd film as well as high magnification images of (b) individual cracks, and (c) points of crack termination. (d) Histograms showing the distribution of nanogap widths and lengths. Note that none of the cracks extend the entire width of the AuPd film (i.e., 3000 $\mu$m). (e) Schematic showing the stress distributions occurring when a bending moment (**M**) is applied to the ends of a sample.



DOI: 10.1021/acssensors.5b00102
*ACS Sens.* 2016, 1, 73−80

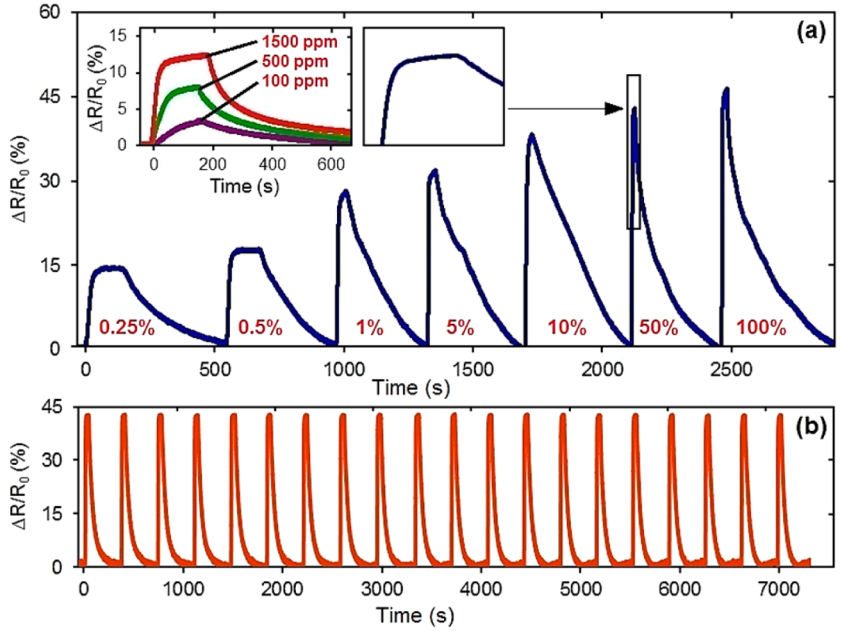


**Figure 3.** (a) Room temperature electrical response of a nanogap sensor as the $H_2$ concentration is varied from 100 ppm to 100%. The two insets show the response at the three lowest concentrations (left) and an expanded view indicating that $H_2$ gas was applied until the signal plateaus (right). (b) Response of a nanogap sensor as it undergoes 20 consecutive $H_2$ on/off cycles at a concentration of 10%.

concentration where the smallest gaps form only near the point of crack closure. The formation of these sub-20 nm nanogaps at the crack tips is significant in that they facilitate the detection of $H_2$ at low concentrations. Forming nanogaps on such small length scales through other means is challenging and has stood as a technological barrier to the development of nanogap sensors with a low detection limit.[11]

Crack formation in the AuPd film results from the tensile stresses originating from the bending deformation. When a material is bent it leads to a stress distribution across its cross section which varies from a maximum compressive stress at the concave surface, to a point of zero stress at the neutral axis, and then to a maximum tensile stress at the convex surface (Figure 2e). At the end of the process, the convex surface has lengthened while the concave surface has shortened. While the actual stress patterns occurring in the four layer device are expected to deviate somewhat from this ideal one layer scenario, they are likely dominated by the steel substrate which is not only the thickest layer, but also has the highest yield strength. When a bending moment (**M**) is applied, the steel will first yield elastically, then plastically, until finally the force is unloaded, the result of which is a partial springback due to elastic strain recovery. A comparison of sensors formed with and without the steel backing reveals that the backing also leads to tensile stresses which crack the AuPd film in a more controlled manner. For this case, nearly all of the cracks run parallel to each other along the width of the sensing element with few intersections. When the backing is absent, numerous cracks run in random directions forming crisscross patterns (Figure S1) which typically lead to a 5-fold increase in the sensor resistance and an overall reduction in sensor-to-sensor reproducibility.

During the bending deformation the Kapton tape plays a substantial role in that it significantly reduces the tensile stress placed on the AuPd film. This is apparent when comparisons are made to an identical film deposited on Teflon, a more rigid polymer, which is then bent to the same radius of curvature; the result is cracking which is far more severe, with both wider gaps and longer cracks (Figure S2). While it is difficult to separate the exact roles of the upper polyimide layer and the underlying adhesive in relieving the tensile stress, there is little doubt that the adhesive lessens the tensile stress placed on the AuPd layer during bending. If the ends of the Kapton tape were held rigidly against the steel then, upon bending, the tape would have to elongate in order to accommodate the estimated 190 $\mu$m increase in the length of the steel at its convex surface (Figure S3). An examination of the Kapton after bending, however, reveals that its length has increased by only 30 $\mu$m, a result which suggests that the tape adhesive slides along the steel surface in order to partially release stress formed at the adhesive−steel interface. The existence of this interfacial slippage was confirmed by examining the position of the tape relative to alignment markers before and after bending. With no obvious loss of bonding between the adhesive and steel backing resulting from this interfacial motion, the slippage plays a positive role in that it safeguards against excessive and erratic crack formation.

**Sensor Operating Principle and Performance.** The sensor operates as a two-probe resistive device responsive to reductions in the AuPd resistance as hydrogen uptake expands the crystal structure and closes the nanogaps. The detection mode, however, differs from standard break-junction nanogap designs in that each nanogap has a range of widths extending up to 200 nm where each width closes at a specific $H_2$ concentration. It should be noted, however, that widest portions of the nanogap may never close since the degree of Pd swelling required is likely unattainable. The overall detection mode is, hence, not restricted to a single on/off sensing modality, but instead shows an overall resistance which steadily falls as the $H_2$ concentration is increased. Similar to other nanogap sensors, the uptake of hydrogen into AuPd also results in changes to its resistivity which contribute to the overall response of the detector. The effect on detector performance is, however, slight since changes to the resistivity


DOI: 10.1021/acssensors.5b00102
*ACS Sens.* 2016, 1, 73−80

are small in comparison to those originating from the closure of nanogaps. The performance of a detector reliant solely on changes to the resistivity (i.e., without nanogaps) is shown in Figure S4 for comparison.

Sensor performance was characterized as a function of $H_2$ concentration expressed as a volumetric percentage (v/v %). Figure 3a shows the electrical response of the sensor defined as the percentage change in resistance normalized to the baseline resistance (i.e., $\Delta R/R_0 \times 100\%$) for $H_2$ concentrations in a range extending from 100 ppm to 100%. With a clear progression in the magnitude of the response as a function of $H_2$ concentration the sensor demonstrates the ability to sense $H_2$ levels over a wide range using the same principle of detection, a capability which has not been previously demonstrated for nanogap sensors. Particularly noteworthy is the fact that the detector response does not saturate at high $H_2$ concentrations. The detector response time does, however, diminish as the $H_2$ concentration is lowered showing values of 1.5, 6, and 120 s for concentrations of 100%, 1%, and 100 ppm, respectively. The sensor recovery time is considerably longer (~400 s) and is not strongly dependent on the $H_2$ concentration. The reversible gas sensing capabilities of the sensors were also assessed. Figure 3b shows the time-dependent response of a similar sensor as it is exposed to 20 consecutive 10% $H_2$ absorption and desorption cycles lasting 30 and 250 s, respectively. It exhibits excellent reversibility, showing no indication of a deterioration in $\Delta R/R_0$ values or in the response and recovery times. Sensors do, however, show an initial cycle (not shown) which is somewhat different from subsequent cycles in that the sensor recovery is incomplete. The lower resistance values (~5%) obtained after the first cycle could be an indication that some degree of irreversible crack healing occurs, where swelling caused by the retention of a small quantities of hydrogen within the AuPd crystal structure may be a contributing factor. The result suggests that precise determination of the $H_2$ concentrations would require that the detector be exposed to $H_2$ prior to use. The potential need for such a sensor conditioning process has been reported previously for other nanogap sensors.[29,38,41,42] The sensitivity of the sensor to changes in the ambient temperature was also evaluated. It indicates that a 15 °C rise in temperature results in a more than 50% decrease in the response and recovery times, but where the $\Delta R/R_0$ value and baseline resistance remain fairly stable (Figure S5).

**Sensor Durability.** Basing a sensing strategy on cracks, a feature which is nominally a material failure mode, raises concerns regarding reliability and durability. While it may seem that sensors formed in this manner are highly susceptible to open circuit failures resulting from a single crack traversing the entire length of the sensor, this is not the case. Of the approximately 30 detectors of various configurations used over the course of this study, none of them have ever shown an open circuit, either after bending or upon repeated exposure to $H_2$. In fact, these sensors have proven quite robust. In order to further assess this issue, the aging characteristics of a single sensor were monitored over a 14 day period, where on each day the sensor was exposed to $H_2$ gas at a 10% concentration. Between tests the sensor was exposed to air. Figure 4 shows that the detector response and its baseline resistance show excellent stability. In addition, an examination of individual cracks before and after 20 on/off $H_2$ cycles at a 10% concentration shows no evidence of crack propagation or alteration (Figure 5). While it is conceded that these aging tests are of short duration in comparison to desirable sensor lifetimes, the results are promising in terms of both maintaining sensor performance and the integrity of the nanogaps.

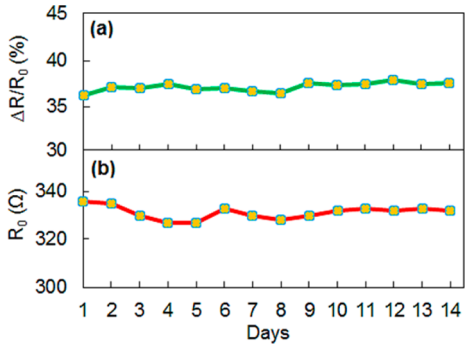


**Figure 4.** Time dependence of the (a) sensor response and (b) its baseline resistance monitored over a 14 day period where on each day the sensor was exposed to $H_2$ at a 10% concentration. Note that the sensor exhibits excellent aging characteristics over this time interval.

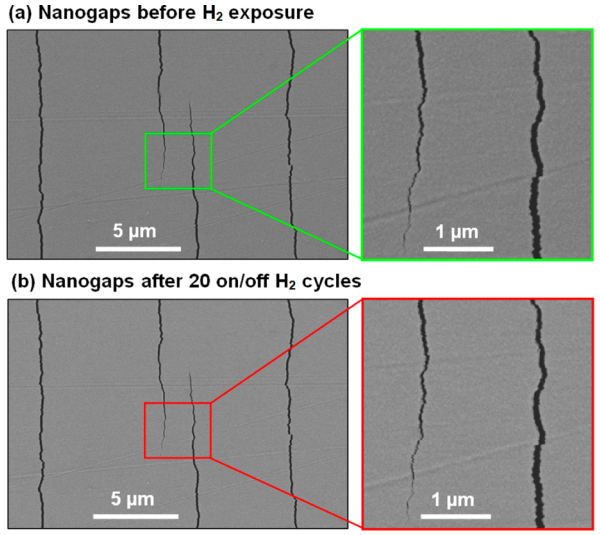


**Figure 5.** SEM images of (a) nanogaps formed through a bending deformation and (b) the same nanogaps after being exposed to 20 on/off $H_2$ cycles with a 10% concentration. The near-identical patterns indicate a high level of crack stability during $H_2$ absorption/desorption cycles.

Sensor durability is most likely due to a combination of stress relieving mechanisms occurring both at the time of nanogap formation and as the AuPd layer swells and contracts during $H_2$ absorption−desorption cycles. During nanogap formation the AuPd layer and Kapton tape are placed under tensile stress. With the aforementioned slippage at the adhesive−steel interface relieving much of the induced tensile stress, the remaining stress must be accommodated through an elongation of the polyimide which, in turn, cracks the AuPd film. An estimation of this elongation, based on the nanogap size distribution, yields a value of 30 $\mu$m. It is, however, unclear how much of this strain remains elastic, i.e., how much has been accommodated by plastic deformation. Regardless, this situation is not conducive to crack stability since it would leave a stress concentration at the crack tip. It should, however, be recognized that this stress concentration is offset by a small contraction in the polyimide which occurs at the end of the bending process when elastic strain is reduced as the bending


DOI: 10.1021/acssensors.5b00102
ACS Sens. 2016, 1, 73−80

force is unloaded and the steel undergoes a small recoil due to elastic strain recovery. As this occurs, crack stability is assured by relieving the stress concentration at the crack tip and a partial closure of the crack. This explanation is consistent with our observation that nanogaps appear closed at the cracks tips without ever being exposed to $H_2$ (Figure 5). The end result is a stable crack tip since the stress concentration is well below that needed for it to propagate. Crack propagation resulting from $H_2$ absorption is also unlikely since it leads to compressive forces which close the cracks. While compressive forces have led to delamination or blistering in other Pd-based $H_2$ sensors,[50] no such occurrences have been observed here, a result which likely stems from the polyimide acting as a compliant polymeric substrate able to effectively offset strains at the incoherent AuPd/polyimide interface in a manner similar to that demonstrated by Kiefer et al.[31,40] and Lee and co-workers.[38,39]

**Overall Assessment of Sensor Characteristics.** The prototyped device capitalizes on recent advances in $H_2$ nanogap sensors which demonstrate the utility of using both a compliant polymeric substrate and Pd alloys as the sensing element. It builds upon these breakthroughs by utilizing a bending deformation to form a continuum of nanogaps which close sequentially as the $H_2$ partial pressure is increased. In doing so, existing hurdles which have impeded the advancement of this sensing platform have been alleviated by (i) expanding the overall range of $H_2$ detection to include concentrations ranging from atmospheric pressure to a 100 ppm, (ii) providing a straightforward means to produce nanogaps with sub-20 nm dimensions, and (iii) devising an inexpensive process for device fabrication with minimal processing requirements. Other advantages of the device include recyclability, high selectivity toward $H_2$, low power consumption, simple circuitry, short wake-up times, and aging characteristics which, while not yet fully validated, are encouraging.

While this sensing strategy shows significant promise, it is not without its shortcomings. Even though each sensor is able to detect $H_2$ gas over a wide range of concentrations, the reproducibility in terms of fabricating sensors with near-identical calibration curves is not yet achievable. A further complication when precise readings are required is the need for device conditioning with $H_2$ gas prior to use. These disadvantages, however, lose significance for applications where constraints on precision are relaxed. A further concern is the substantial increase in response and recovery times which occur as the $H_2$ concentration is lowered. It should be noted that much faster response and recovery times are likely attainable by reducing the AuPd film thickness[31] or operating the device at higher temperatures.[52,53] Polyimide, being a thermosetting polymer, should be amenable to higher operating temperatures.[40] It is also acknowledged that sensor performance, which was demonstrated using an inert carrier gas, may be significantly altered when operated in air.[54,55] Another potential downside is the somewhat larger footprint which the three-dimensional sensor has in comparison to the more compact planar format of most nanogap sensors. It should, however, be recognized that miniaturization of the sensing element is a possibility and that the sensing element, even in its current form, is still relatively small when compared to the size of a typical hand-held sensing device. In general, the parameter space for this detection strategy has not yet been fully explored and, as such, is expected to offer significant improvements once optimized.

## CONCLUSION

We have demonstrated a two terminal resistive nanogap sensing device able to operate at room temperature and sense $H_2$ gas at concentrations ranging from 100 ppm to 1 atm. The prototyped device derives novelty from a single-step bending deformation which is used to define a continuum of nanogaps which allows for a detection mode which is reliant on their collective response. The devised detection strategy not only advances a promising sensing platform toward full-range $H_2$ detection, but also provides the impetus to adapt it to a growing set of analytes which are amenable to nanogap sensing technologies.

## ASSOCIATED CONTENT

### Supporting Information

The Supporting Information is available free of charge on the ACS Publications website at DOI: 10.1021/acssensors.5b00102.

SEM images of sensors with various backing layers; schematic representation of a bending deformation; operating characteristics of a resistivity-based AuPd sensor; and temperature dependence of a nanogap sensor (PDF)

## AUTHOR INFORMATION


### Corresponding Author

*E-mail: neretina@temple.edu.


### Notes

The authors declare no competing financial interest.

## ACKNOWLEDGMENTS

This work is funded by the National Science Foundation (DMR-1053416) CAREER Award to S. Neretina. The work has benefited from the facilities available through Temple University's Nano Instrumentation Center, which is based on DoD DURIP Award N0014-12-1-0777 from the Office of Naval Research and is sponsored by the College of Engineering. The authors also acknowledge helpful discussions with Dr. Robert J. Ryan (College of Engineering, Temple University).

## REFERENCES


(1) Hübert, T.; Boon-Brett, L.; Black, G.; Banach, U. Hydrogen Sensors - A Review. *Sens. Actuators, B* **2011**, *157*, 329−352.

(2) Buttner, W. J.; Post, M. B.; Burgess, R.; Rivkin, C. An Overview of Hydrogen Safety Sensors and Requirements. *Int. J. Hydrogen Energy* **2011**, *36*, 2462−2470.

(3) Tachibana, Y.; Vayssieres, L.; Durrant, J. R. Artificial Photosynthesis for Solar Water-Splitting. *Nat. Photonics* **2012**, *6*, 511−518.

(4) Ahmad, H.; Kamarudin, S. K.; Minggu, L. J.; Kassim, M. Hydrogen from Photo-Catalytic Water Splitting Process: A Review. *Renewable Sustainable Energy Rev.* **2015**, *43*, 599−610.

(5) Peter, L. M. Photoelectrochemical Water Splitting. A Status Assessment. *Electroanalysis* **2015**, *27*, 864−871.

(6) Zou, X.; Zhang, Y. Noble Metal-Free Hydrogen Evolution Catalysts for Water Splitting. *Chem. Soc. Rev.* **2015**, *44*, 5148−5180.

(7) Hisatomi, T.; Kubota, J.; Domen, K. Recent Advances in Semiconductors for Photocatalytic and Photoelectrochemical Water Splitting. *Chem. Soc. Rev.* **2014**, *43*, 7520−7535.

(8) Wang, W.; Wang, S.; Ma, X.; Gong, J. Recent Advances in Catalytic Hydrogenation of Carbon Dioxide. *Chem. Soc. Rev.* **2011**, *40*, 3703−3727.




DOI: 10.1021/acssensors.5b00102
*ACS Sens.* 2016, 1, 73−80

(9) Izumi, Y. Recent Advances in the Photocatalytic Conversion of Carbon Dioxide to Fuels with Water and/or Hydrogen using Solar Energy and Beyond. *Coord. Chem. Rev.* **2013**, *257*, 171−186.
(10) Li, Y.; Chan, S. H.; Sun, Q. Heterogenious Catalytic Conversion of $CO_2$: A Comprehensive Theoretical Review. *Nanoscale* **2015**, *7*, 8663−8683.
(11) Lee, J.; Shim, W.; Noh, J.-S.; Lee, W. Design Rules for Nanogap-Based Hydrogen Gas Sensors. *ChemPhysChem* **2012**, *13*, 1395−1403.
(12) Arya, S. K.; Krishnan, S.; Silva, H.; Jean, S.; Bhansali, S. Advances in Materials for Room Temperature Hydrogen Sensors. *Analyst* **2012**, *137*, 2743−2756.
(13) Wadell, C.; Syrenova, S.; Langhammer, C. Plasmonic Hydrogen Sensing with Nanostructured Metal Hydrides. *ACS Nano* **2014**, *8*, 11925−11940.
(14) Gu, H.; Wang, Z.; Hu, Y. Hydrogen Gas Sensors Based on Semiconductor Oxide Nanostructures. *Sensors* **2012**, *12*, 5517−5550.
(15) Boon-Brett, L.; Bousek, J.; Black, G.; Moretto, P.; Castello, P.; Hubert, T.; Banach, U. Identifying Performance Gaps in Hydrogen Safety Sensor Technology for Automotive and Stationary Applications. *Int. J. Hydrogen Energy* **2010**, *35*, 373−384.
(16) Potje-Kamloth, K. Semiconductor Junction Gas Sensors. *Chem. Rev.* **2008**, *108*, 367−399.
(17) Korotcenkov, G.; Han, S. D.; Stetter, J. R. Review of Electrochemical Hydrogen Sensors. *Chem. Rev.* **2009**, *109*, 1402−1433.
(18) Hübert, T.; Boon-Brett, L.; Palmisano, V.; Bader, M. A. Developments in Gas Sensor Technology for Hydrogen Safety. *Int. J. Hydrogen Energy* **2014**, *39*, 20474−20483.
(19) Favier, F.; Walter, E. C.; Zach, M. P.; Benter, T.; Penner, R. M. Hydrogen Sensors and Switches from Electrodeposited Palladium Mesowire Arrays. *Science* **2001**, *293*, 2227−2231.
(20) Sil, D.; Gilroy, K. D.; Niaux, A.; Boulesbaa, A.; Neretina, S.; Borguet, E. Seeing is Believing: Hot Electron based Gold Nanoplasmonic Optical Hydrogen Sensor. *ACS Nano* **2014**, *8*, 7755−7762.
(21) Wadell, C.; Nugroho, F. A. A.; Lidstrom, E.; Iandolo, B.; Wagner, J. B.; Langhammer, C. Hysteresis-Free Nanoplasmonic Pd−Au Alloy Hydrogen Sensors. *Nano Lett.* **2015**, *15*, 3563−3570.
(22) Gilroy, K. D.; Sundar, A.; Hajfathalian, M.; Yaghoubzade, A.; Tan, T.; Sil, D.; Borguet, E.; Hughes, R. A.; Neretina, S. Transformation of Truncated Gold Octahedrons into Triangular Nanoprisms through the Heterogeneous Nucleation of Silver. *Nanoscale* **2015**, *7*, 6827−6835.
(23) Sil, D.; Udeoyo, U.; Hines, J.; Borguet, E. Palladium Nanoparticle-Based Surface Acoustic Wave Hydrogen Sensor. *ACS Appl. Mater. Interfaces* **2015**, *7*, 5709−5714.
(24) Huang, F.-C.; Chen, Y.-Y.; Wu, T.-T. A Room Temperature Surface Acoustic Wave Hydrogen Sensor with Pt Coated ZnO Nanorods. *Nanotechnology* **2009**, *20*, 065501.
(25) Jakubik, W. P.; Urbanczyk, M. W.; Kochowski, S.; Bodzenta, J. Palladium and Phthalocyanine Bilayer Films for Hydrogen Detection in a Surface Acoustic Wave Sensor System. *Sens. Actuators, B* **2003**, *96*, 321−328.
(26) Lange, U.; Hirsch, T.; Mirsky, V. M.; Wolfbeis, O. S. Hydrogen Sensor based on a Graphene-Palladium Nanocomposite. *Electrochim. Acta* **2011**, *56*, 3707−3712.
(27) Wang, J.; Singh, B.; Park, J. H.; Rathi, S.; Lee, I.-Y.; Maeng, S.; Joh, H.-I.; Lee, C.-H.; Kim, G.-H. Dielectrophoresis of Graphene Oxide Nanostructures for Hydrogen Gas Sensor at Room Temperature. *Sens. Actuators, B* **2014**, *194*, 296−302.
(28) Lee, J. H.; Kang, W.-S.; Najeeb, C. K.; Choi, B.-S.; Choi, S.-W.; Lee, H. J.; Lee, S. S.; Kim, J.-H. A Hydrogen Gas Sensor using Single-Walled Carbon Nanotube Langmuir-Blodgett Films Decorated with Palladium Nanoparticles. *Sens. Actuators, B* **2013**, *188*, 169−175.
(29) Walter, E. C.; Favier, F.; Penner, R. M. Palladium Mesowire Arrays for fast Hydrogen Sensors and Hydrogen-Actuated Switches. *Anal. Chem.* **2002**, *74*, 1546−1553.
(30) Hughes, R. C.; Schubert, W. K. Thin-Films of Pd/Ni Alloys for Detection of High Hydrogen Concentrations. *J. Appl. Phys.* **1992**, *71*, 542−544.
(31) Kiefer, T.; Favier, F.; Vazquez-Mena, O.; Villanueva, G.; Brugger, J. A Single Nanotrench in a Palladium Microwire for Hydrogen Detection. *Nanotechnology* **2008**, *19*, 125502.
(32) Zhao, M.; Wong, M. H.; Ong, C. W. Achievement of Controlled Resistive Response of Nanogapped Palladium Film to Hydrogen. *Appl. Phys. Lett.* **2015**, *107*, 033108.
(33) Jebril, S.; Elbahri, M.; Titazu, G.; Subannajui, K.; Essa, S.; Niebelschütz, F.; Röhlig, C.-C.; Cimalla, V.; Ambacher, O.; Schmidt, B.; Kabiraj, D.; Avasti, D.; Adelung, R. Integration of Thin-Film-Fracture-Based Nanowires into Microchip Fabrication. *Small* **2008**, *4*, 2214−2221.
(34) van Megan, M. J. J.; Olthuis, W.; van den Berg, A. Solid State Nanogaps for Electrochemical Detection Fabricated using Edge Lithography. *Microelectron. Eng.* **2014**, *115*, 21−25.
(35) Kiefer, T.; Salette, A.; Villanueva, L. G.; Brugger, J. Large Arrays of Chemo-Mechanical Nanoswitches for Ultralow-Power Hydrogen Sensing. *J. Micromech. Microeng.* **2010**, *20*, 105019.
(36) Mubeen, S.; Yoo, B.; Myung, N. V. Fabrication of Nanoelectrodes and Nanojunction Hydrogen Sensor. *Appl. Phys. Lett.* **2008**, *93*, 133111.
(37) Dasari, R.; Zamborini, F. P. Hydrogen Switches and Sensors Fabricated by Combining Electropolymerization and Pd Electrodeposition at Microgap Electrodes. *J. Am. Chem. Soc.* **2008**, *130*, 16138−16139.
(38) Lee, J.; Shim, W.; Lee, E.; Noh, J.-S.; Lee, W. Highly Mobile Palladium Thin Films on an Elastomeric Substrate: Nanogap-Based Hydrogen Gas Sensors. *Angew. Chem., Int. Ed.* **2011**, *50*, 5301−5305.
(39) Lee, J.; Noh, J.-S.; Lee, S. H.; Song, B.; Jung, H.; Kim, W.; Lee, W. Cracked Palladium Films on an Elastomeric Substrate for Use as Hydrogen Sensors. *Int. J. Hydrogen Energy* **2012**, *37*, 7934−7939.
(40) Kiefer, T.; Villanueva, L. G.; Fargier, F.; Favier, F.; Brugger, J. Fast and Robust Hydrogen Sensors Based on Discontinuous Palladium Films on Polyimide, Fabricated on a Wafer Scale. *Nanotechnology* **2010**, *21*, 505501.
(41) Moon, H. M.; Myung, N. V.; Haberer, E. D. Chemiresistive Hydrogen Gas Sensors from Gold-Palladium Nanopeapods. *Appl. Phys. Lett.* **2014**, *105*, 223102.
(42) Cherevko, S.; Kulyk, N.; Fu, J.; Chung, C.-H. Hydrogen Sensing Performance of Electrodeposited Conoidal Palladium Nanowire and Nanotube Arrays. *Sens. Actuators, B* **2009**, *136*, 388−391.
(43) Wagner, S.; Hamm, M.; Pundt, A. Huge Hydrogen-Induced Resistive Switching in Percolating Palladium Thin Films. *Scr. Mater.* **2013**, *69*, 756−759.
(44) Khanuja, M.; Kala, S.; Mehta, B. R.; Kruis, F. E. Concentration-Specific Hydrogen Sensing Behavior in Monosized Pd Nanoparticle Layers. *Nanotechnology* **2009**, *20*, 015502.
(45) Noh, J.-S.; Kim, H.; Kim, B. S.; Lee, E.; Cho, H. H.; Lee, W. High-Performance Vertical Hydrogen Sensors using Pd-Coated Rough Si Nanowires. *J. Mater. Chem.* **2011**, *21*, 15935−15939.
(46) Ohara, S.; Hatakeyama, Y.; Umetsu, M.; Sato, K.; Naka, T.; Adschiri, T. Palladium-Polelectrolyte Hybrid Nanoparticles for Hydrogen Sensor in Fuel Cells. *J. Power Sources* **2009**, *193*, 367−370.
(47) van Lith, J.; Lassesson, A.; Brown, S. A.; Schulze, M.; Partridge, J. G.; Ayesh, A. A Hydrogen Sensor Based on Tunneling Between Palladium Clusters. *Appl. Phys. Lett.* **2007**, *91*, 181910.
(48) Kim, K. T.; Sim, S. J.; Cho, S. M. Hydrogen Gas Sensor Using Pd Nanowires Electro-Deposited Into Anodized Alumina Template. *IEEE Sens. J.* **2006**, *6*, 509−513.
(49) Xu, T.; Zach, M. P.; Xiao, Z. L.; Rosenmann, D.; Welp, U.; Kwok, W. K.; Crabtree, G. W. Self-Assembled Monolayer-Enhanced Hydrogen Sensing with Ultrathin Palladium Films. *Appl. Phys. Lett.* **2005**, *86*, 203104.
(50) Lee, E.; Lee, J. M.; Koo, J. H.; Lee, W.; Lee, T. Hysteresis Behavior of Electrical Resistance in Pd Thin Films during the Process of Absorption and Desorption of Hydrogen Gas. *Int. J. Hydrogen Energy* **2010**, *35*, 6984−6991.
(51) McKinley, D. L. Metal Alloy for Hydrogen Separation and Purification. US Patent 3,350,845, 1967.


DOI: 10.1021/acssensors.5b00102
*ACS Sens.* 2016, 1, 73−80

(52) Yang, F.; Taggart, D. K.; Penner, R. M. Joule Heating a Palladium Nanowire Sensor for Accelerated Response and Recovery to Hydrogen Gas. *Small* **2010**, *6*, 1422−1429.
(53) Wang, M.; Feng, Y. Palladium-Silver Thin Film for Hydrogen Sensing. *Sens. Actuators, B* **2007**, *123*, 101−106.
(54) Sun, Y.; Wang, H. H.; Xia, M. Single-Walled Carbon Nanotubes Modified with Pd Nanoparticles: Unique Building Blocks for High Performance, Flexible Hydrogen Sensors. *J. Phys. Chem. C* **2008**, *112*, 1250−1259.
(55) Ou, Y. J.; Si, W. W.; Yu, G.; Tang, L. L.; Zhang, J.; Dong, Q. Z. Nanostructures of Pd-Ni Alloy Deposited on Carbon Fibers for Sensing Hydrogen. *J. Alloys Compd.* **2013**, *569*, 130−135.



DOI: 10.1021/acssensors.5b00102
*ACS Sens.* 2016, 1, 73−80